UV and aging effect on the degradation of PEDOT:PSS/nSi films for Hybrid Silicon solar cells

Antonio Vázquez-López,[a,b] Marina García Carrión [a], David Maestre,[a] , Smagul Zh, Karazhanov,[c] Erik.S. Marstein [c], Bianchi Méndez, [a] Ana Cremades[a]

[a]*Department of Materials Physics, Faculty of Physics, Complutense University of Madrid, 28040 Madrid, Spain*

[b]*IMDEA Materials Institute, C/Eric Kandel, 2, Getafe, Madrid 28906, Spain*

[c]*Department for Solar Energy, Institute for Energy Technology, 2027 Kjeller, Oslo, Norway*

Keywords: PEDOT:PSS, degradation, PLQSSPC, etching, UV-irradiation, Hybrid Silicon solar cells

email: antvaz01@ucm.es

Abstract:

Poly(3,4-ethylene-dioxythiophene):poly(styrenesulfonate) (PEDOT:PSS) is one of the most successful conductive polymers, key component in different organic-based devices including silicon Hybrid Solar Cells (HSCs). However, there is limited information so far about the stability of this polymer under operation scenarios similar to those employed during performance, including UV irradiation or storage time. In this work, PEDOT:PSS thin layers have been spin coated onto silicon substrates, and their stability has been analysed under different conditions. Firstly, the influence under laser irradiation has been studied by Raman spectroscopy using both an UV-laser of 325 nm and a VIS-laser of 633 nm, with variable irradiation intensities and exposure time. Secondly, the effect of the removal of the native silicon oxide layer on the silicon substrate on the stability and passivation performance of the PEDOT:PSS has been analysed. Lastly, and closely related to its application in HSCs, the photoluminescence recombination has been analysed over storage time for 2 months to evaluate their real implementation as long-lasting solar cells.

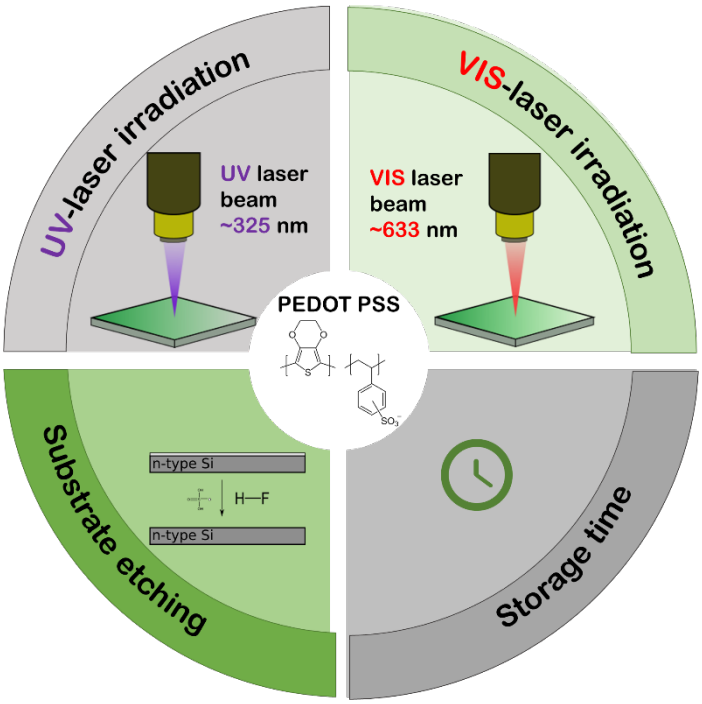

1. Introduction

PEDOT:PSS (poly(3,4-ethylene-dioxythiophene):poly(styrenesulfonate)) is considered one of the most successful conductive polymers (CP) to date. It has found application in several organic electro-optical devices, mainly due to its properties: transparency in the visible range (~ 90% between 400-700 nm), good p-type electrical conductivity and superior carrier mobility [1], among others. PEDOT:PSS is currently commercially available with different mass ratios and properties, being the so-called PH1000 distributed by Clevios™, one of the most successful so far [1,2], particularly in the field of silicon hybrid solar cells (HSCs) [3–8] reaching power conversion efficiencies up to 14.8% [9]. Different approaches have been proposed so far to improve PEDOT:PSS performance as part of HSCs by increasing the lifetime recombination, electrical conductivity, surface wettability, stability and remarkably by the use of additives [1,10] such as Dimethyl Sulfoxide (DMSO) [11–13] and surfactants such as Triton X-100[14–16]. The concentration of these additives varies concerning the desired outcome. As some examples, 5% DMSO[11] has shown the best results in terms of conductivity, while Triton X-100 concentration varies

from 0.1[14], 3[15] or 10%[16] showing improved electrical properties with lower concentrations and improved mechanical properties with increasing concentration.

As pointed out on the literature [3,9,17] PEDOT:PSS has been also used as front contact for silicon heterojunction solar cells conforming hybrid solar cells (HSCs), with potential to achieve comparable efficiency to conventional Si homojunction[8]. Besides, different works have pointed out that PEDOT:PSS is a good passivation layer for Si, as well [3,4,9,18,19]. Chen at al.[18] demonstrated that the passivation of the Si surface is mostly due to the oxidation at the PSS/Si interface which can be controlled by electron transfer. PEDOT:PSS/nSi forms a p-n junction dominated by the diffusion of minority charge carriers[9,20] where the silicon surface and the interplay of PEDOT:PSS/nSi play key roles on the performance. Usually, Si wafers present a layer of the native/grown SiO_x which might interfere on the recombination processes. Recently, it has been suggested that this layer can grow over time[20], even after PEDOT:PSS deposition, thus its removal using chemical etching can be considered as a way-to-go to improve the photovoltaic performance. In that sense, fundamental knowledge on the evolution of recombination lifetime over time or the effect of the silicon oxide layer on performance still remain understudied.

While increasing efficiencies are obtained experimentally, scarce research can be found so far focused on their real implementation as long-lasting devices. Indeed, one major issue that HSCs face is degradation under operation, as HSCs usually face adverse environment under working conditions. It is accepted that the dominant degradation mechanism in air is the itself degradation of the polymeric chains under oxygen and moisture ambient [20], but other effects such as the stability of the n-Si/PEDOT:PSS interface might also represent another degradation focus. Also, organic polymers are sensitive to other factors, such as adverse atmosphere conditions, high gas concentrations, humidity, extreme outdoor temperatures and continuous UV-C irradiation. All these factors will affect its performance as well as decrease its total lifetime expectancy. To date, PEDOT:PSS stability has been studied by different authors [21–23] such as Vitoratos et al. which showed the relation between electrical conductivity (σ) and thermal treatments [24]

as well as under variable atmospheres [25]. Nonetheless, stability under UV or VIS irradiation as well as the role of the silicon oxide layer on the optoelectronic properties remain considerably understudied, despite the relevance of these aspects in the final performance of the polymer-based device. Similarly, studies on other key parameters for solar cell performance, such as carrier lifetime (τ), which is expected to change over time, are also scarce. In that sense, higher carrier lifetime will imply a longer recombination time, and therefore will affect the solar cell efficiency [5]. It is important to mention that degradation issue of PEDOT:PSS has been considered for other polymer-based applications such as thermoelectric [21,26], battery electrodes [27] or micro-electrochemical energy storage (MEES) [28], where the insights achieved in the degradation mechanisms can led to improved performance and significant advances in those fields of research.

In this work, we report on the stability and aging process on PEDOT:PSS thin films assembled via spin coating based on PEDOT:PSS/DMSO/TritonX-100 composites under different conditions. Firstly, we show the modifications under laser irradiation (UV- and Vis- laser irradiation) over variable periods of time, as well as irradiation intensities. Then, we focus our study on the variations on the recombination lifetimes of the PEDOT:PSS-based composites and the effect observed by the pre-treatment of the silicon surface (the PEDOT:PSS/nSi interface) and aging over time, obtained by PL-QSSPC (Photoluminescence Quasi-steady state photoconductance) technique.

2. Experimental section

2.1 Materials and methods

PEDOT:PSS (Clevios M122, PH 1000, solid content 1.0–1.3%) was purchased from Ossila. Dimethyl sulfoxide (DMSO) (Sigma Aldrich) was added in 5 wt% [11,12] to the polymer to improve electrical conductivity, while for the achievement of better surface wettability Triton X-100 was added in 0.1 wt% to the mixture. The obtained solution was magnetically stirred and filtered with a Polyethersulfone (PES)

membrane (0.45 μm porosity). Hereinafter, PEDOT:PSS will be used to name these samples, which also include DMSO and Triton X-100 as additives.

2.2 Fabrication of PEDOT:PSS thin films

The mixture was spin-coated by using a pipettor 150 μL of the PEDOT:PSS mixture placed ~2 cm over the substrate and was manually poured through the spinning substrate. The substrate then was left spinning at 6000 rpm during 50 s, which creates a thin homogeneous layer. After 50s, the speed of the substrate is decreased until stoppage.

The employed substrates were silicon n-type float-zone (FZ) (FZ, TOPSIL, thickness 280 ± 20 nm) as described in [5–7] either without any treatment or chemically treated to remove the native oxide layer. To remove this oxide layer, when necessary, the wafer was introduced into a mixture of HF and distilled water (1:8) during 30 s and then rinsed with water. Secondly, sulfuric acid (H_2SO_4) and hydrogen peroxide (H_2O_2) were mixed into a beaker (commonly refereed as Piranha solution) with a ratio of 4:1 (1L of sulfuric acid per 250 mL of hydrogen peroxide). The reaction is strongly exothermic and abruptly rises to boiling temperature which was maintained at 100ºC with aid of a hot plate. Each silicon wafer was introduced on the beaker for 30 min. Finally, it was rinsed with water and carefully dried with a flow of nitrogen gas.

Glass substrates were also used, mainly for optical measurements. The circular substrates were cut into four same-size pieces, with a radius of 5 cm. The selected glass substrates were previously treated with isopropanol and boiling water and dried with N_2. For both silicon and glass substrates after the coating samples were placed over a substrate for 120°C during 15 min to evaporate any remaining moisture. For aging studies, samples were placed on darkness on a storage room.

2.3 Characterization

Secondary Electron images were recorded by a FEI Inspect SEM while energy dispersive x-ray spectroscopy (EDS) was obtained using a Bruker AXS Quantax system attached to a Leica 440 SEM

working between 10-15 kV. UV-VIS Optical absorption was measured with a UV-vis-NIR light source DH-200 ocean optics with a Deuterium and Halogen lamp. Raman spectroscopy measurements were carried out at room temperature on a Horiba Jobin-Yvon LabRam Hr800 (Horiba, Kyoto, Japan) using both continuous wave He-Ne laser (λ = 633 nm) and He-Cd laser (λ = 325 nm). Raman was calibrated using the 520 cm^{-1} mode of Silicon. Different neutral filters were used to attenuate the total laser intensity, when necessary, diminishing the laser intensity from the nominal 5 mW or 13 mW (I_0), respectively, for the UV or red laser to approximately $0.5 \cdot I_0$ (D_{03}), $0.25 \cdot I_0$ (D_{06}), $0.1 \cdot I_0$ (D_1), or $0.01 \cdot I_0$ (D_2) with the use of neutral filters. The laser was focused onto the sample surface using a 40× objective (numerical aperture = 0.5, Thorlabs LMU-40X-NUV), which led to a laser spot diameter around 1 μm for the UV laser and a few microns for the red laser. The scattered light was collected with the same objective and dispersed with a grating of 2400 L/mm for UV and 600 L/mm for VIS and finally acquired with an air-cooled CCD detector Synapse. Photoluminescence Quasi-steady state photoconductance (PLQSS-PC) measurements were carried out using a BT Imaging LIS-R1 with a laser (λ = 808 nm) at constant illumination intensity of 4.2×10^{-2} W cm^{-2}.

3. Results and discussion

3.1 PEDOT:PSS thin layers characterization

After obtaining the thin layers by means of spin coating, the thickness of the PEDOT:PSS layers was estimated by introducing the samples into the SEM chamber, placed at normal incidence with respect to the electron beam. In this configuration, the interlayer of PEDOT:PSS/nSi and the electron beam are perpendicular to each other. To obtain a reliable measurement, samples were cut forming a 1.5×1.5 cm^2 square from its original size, which was a quarter of the circular wafer which can be observed in Fig S1, in order to avoid artifacts during the thickness measurement, such as the possible bending of the PEDOT:PSS layer over the edge of the silicon wafer. The SEM micrograph can be observed at Fig. 1(a). After various measurements, averaged thickness around 150 nm was obtained, as marked by the red dot in the corresponding box diagram shown in Fig.1(b), where each measurement is represented by a blue dot

and the blue line indicates the data dispersion values. It should be noted that the sample might be ±1-2º degrees tilted, so the thickness results have an inherent uncertainty, however, the PEDOT:PSS films exhibits good coverage of the Si substrate and homogeneous thickness. From the EDS analysis shown in Fig. 1(c)-(d), only signal from the of S, C and O are present, as expected for PEDOT:PSS, as well as Si from the substrate. For measuring the optical behaviour of the samples, PEDOT:PSS was spin coated onto glass substrates. The samples show a high transparency in the visible region, as observed in Fig. 1(e). From the absorption spectra (not show here), the Tauc-plot was calculated (inset in Fig. 1(e)), which leads to an estimation of the optical bandgap value around 3.6 eV, in agreement with previous reports[29].

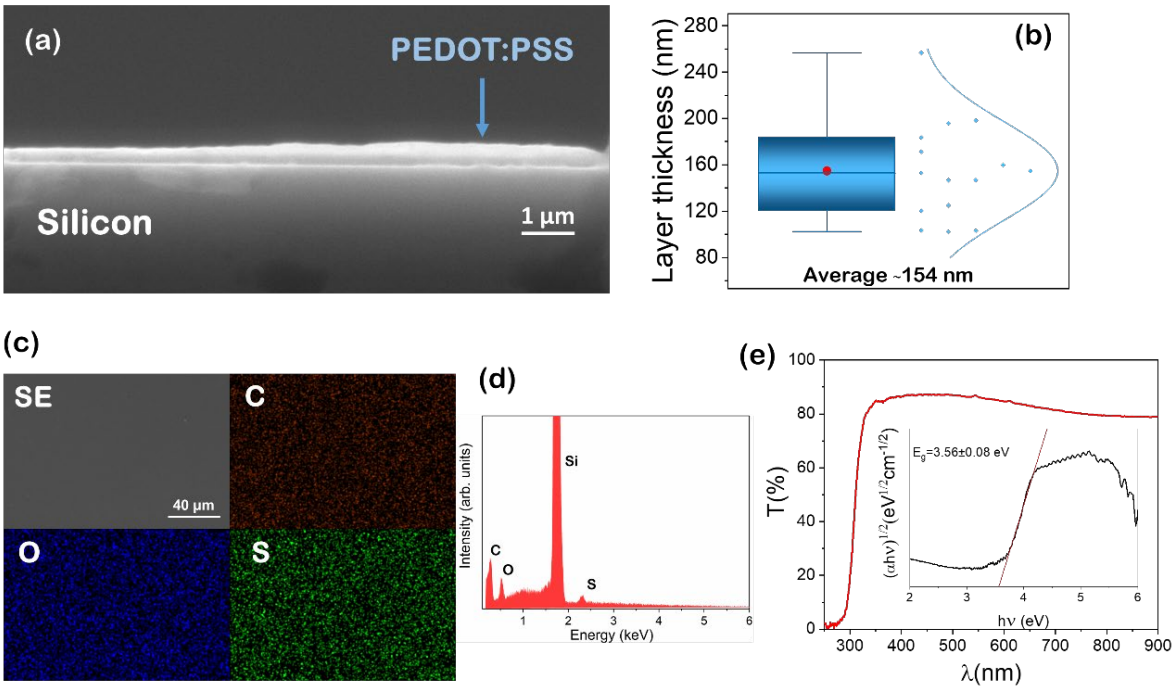

Fig. 1: (a) SEM micrograph acquired at normal incidence on the silicon substrate (b) estimated thickness of the PEDOT:PSS layer measured by averaging the thicknesses observed in different zones. Red dot shows the average thickness. (c) EDS mapping of PEDOT:PSS with its corresponding element mappings labelled on each image (SE: Secondary Electrons, C: Carbon, O: Oxygen and S: Sulphur) and (d) a representative EDS spectrum. (e) Transmittance spectrum of PEDOT:PSS. Inset in (e) shows Tauc-plot obtained from the absorption spectrum.

3.2 Stability study under laser irradiation

Variable irradiation excitation source, duration and intensities were employed during the acquisition of the Raman spectra from PEDOT:PSS/n-type Si, aiming for analysing the stability upon irradiation of the samples under study.

3.2.1 VIS laser

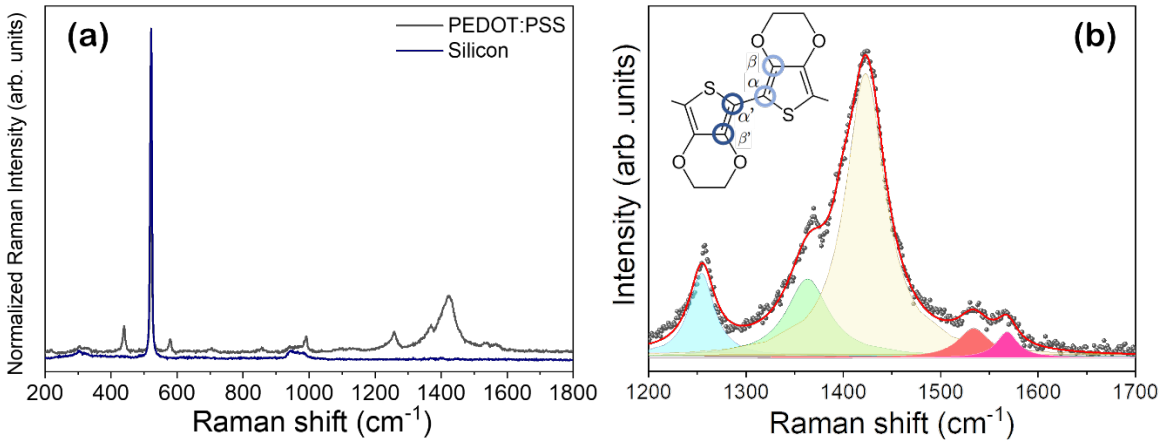

Fig. 2 : Raman spectrum of the PEDOT:PSS acquired with a red laser (λ =633 nm) and a pinhole of 200 μm. Raman spectrum from bare Si substrate (n-type FZ) is also included in (a) as a reference. (b) shows deconvolutions to Gaussian-Lorentz functions of the region between 1200 cm^{-1} and 1700 cm^{-1} corresponding to Raman spectrum from PEDOT:PSS in (a). Inset shows PEDOT structure and nomenclature based on the position of the carbon atoms relative to the sulphur atom.

A red laser (λ = 633 nm) was initially used as excitation source, while different pinhole sizes of 200-900μm and a D_1 filter ($0.1 \cdot I_0$) were employed in order to obtain variable irradiation densities. In that sense, the possible degradation induced by laser irradiation as a function of time can be determined by means of the analysis of the PEDOT:PSS vibrational modes upon laser irradiation.

As shown in the Raman spectra in Fig.2, the complete set of vibrational modes can be attributed to PEDOT or PSS ionomers or to the Silicon substrate, as a Raman spectrum from bare Si is also shown in Fig.2(a) as a reference. Raman spectrum from Silicon shows a well-known intense peak at 520 cm^{-1} which corresponds to the transverse optical(TO) mode [30], a broad peak which can be attributed to the

longitudinal acoustic (LA) mode at 300 cm^{-1} and other broad peak at 920-1000 cm^{-1} attributed to Si-O bonds[31] or to the second transverse optical phonon model (2TO)[30]. The remaining Raman modes, mostly attributed to PEDOT ionomer, are listed in Table 1. Note that for most of the literature, the laser used for measuring PEDOT:PSS may vary, which can explain shifts on the measured values and those reported in the literature, as the Raman signal depends on the excitation source. Besides, higher pinhole involves increased excitation density during laser irradiation, which can also modify the Raman signal. Hence, those aspects should be considered during the analysis of the Raman signal. In this work, the main vibrational modes of PEDOT:PSS measured with the red laser (λ=633 nm) are concentrated in the region between 1000 and 1800 cm^{-1} (as shown in Fig.2). Observed modes are in agreement with previous reports both experimental and simulated [32–34]. Outside this region other modes are also observed at ~ 439 cm^{-1}, ~ 578 cm^{-1} , ~ 706 cm^{-1}, ~ 855 cm^{-1}, ~ 988 cm^{-1} the relative intensity of which does not vary significantly when using different pinhole size, commonly reported for PEDOT [34,35]. The most relevant region of study is between 1000-1800 cm^{-1}[7,13,35–39], shown in in Fig.2 (b). In this region we can observe a main contribution around 1424 cm^{-1}, related with C_α=C_β symmetric stretching vibrations. Usually, contribution ~1430 cm^{-1} can be divided into two regions originating from benzoid (neutral structure) and quinoidic structures. The benzoidic form is related to the signal at ~ 1440 cm^{-1} while quinoidic (oxidized structure) signal appears at ~ 1410 cm^{-1} whose chemical structure is presented (Fig. S2). These two structures involve different electrical properties. Actually, it is commonly reported that the quinoid structure results in an enhancement of the electrical conductivity. The relative intensity of the quinoidic signal increases with the DMSO content, as reported by Hwang et al. [13], as the polar solvent leads to changes in the molecular arrangement of the PEDOT and PSS chains by decreasing the Coulomb interactions. It should be noticed that in the scientific literature in some cases there is no specification on the laser conditions used to acquire some of these measurements as well as the DMSO content, which might differ from 5%, which can hinder the analysis and lead to misleading conclusions.

This can be observed by using for instance, a higher pinhole size, as observed in Fig. S3 (a)-(b). With the pinhole size of 200 μm, the main contribution was peaked at 1420 cm^{-1} (yellow in Fig.2(b)). With the 900 μm pinhole, we can observe two main contributions placed at 1400 cm^{-1} and 1429 cm^{-1} (Fig. S3(b)). This two bands are related to the vibration of the benzoid (neutral) structure and related to the quinoid (oxidized) structure [35,40], at lower and higher wavenumber respectively. It is also clearly observed a shoulder at 1500 cm^{-1} (light purple, Fig S3(b)), which could be associated with C_α=C_β asymmetric stretching vibrations [13,34], only observed under this measuring conditions such as under irradiation[41]. In fact, the region at 1400-1500 cm^{-1} appears to be very sensitive to measuring conditions. Almeida et al. reported multiple modes in this region [34], related to the state of reduction-oxidation of the polymer. These findings indicate that with the use of a higher pinhole, PEDOT tends to get oxidized. Therefore, measuring conditions can affect the oxidation state of PEDOT as well as the interpretation of the results concerning the assignation of the Raman modes, so especial care should be taken during the performance of those measurements.

Table 1: Raman modes of PEDOT:PSS between 1200 and 1800 cm^{-1} observed with the VIS red laser (λ = 633) nm where measurements obtained with a 200 μm or a 900 μm pinhole are marked with (†) and (‡), respectively. Positions of the vibrational modes reprinted from the scientific literature are shown for comparison, which were acquired with wavelengths of (λ = 632 nm, He-Ne laser) [36,37], 532 nm[39], 785 nm[35] and 1064 [34] or unspecified[13,38]. The corresponding attributed origins are also included. Graphical representation of each mode can be observed elsewhere [33].

Wavenumber cm^{-1}		
This work	**Literature**	**Attributed origin**
578	578[35], 578 [34]	PEDOT Oxyethylene ring deformation
706	699[35], 703 [34]	PEDOT Symmetric C–S–C deformation
988	988[35], 989 [34]	PEDOT Oxyethylene ring deformation
1120† ,1111‡	1097[35],1100[13]	PEDOT C–O–C deformation or PSS
1257† , 1254‡	1269[39],1253[13], 1270[36] 1256[37]	C_α-C_α' inter-ring stretching, C_β-H bending
1363† ,1365‡	1361[37] 1368[38],1369[39],1366[13], 1370[36]	single C_β-C_β' stretching vibration
1424† , 1400‡ &1429‡	1424[39],1431[35],1435[13] 1430 [36],1440[36]	C_α=C_β symmetric stretching vibrations
1499‡	1508[38],1504[37], 1490[13]	C_α=C_β Asymmetric stretching vibration
1534† , 1530‡	1530[36],1532[13],1540[38] 1534[37]	Arises from the splitting of the C_α=C_β asymmetric vibrations
1568† , 1561‡	1568[38] [37],1575[39]	C_α=C_β asymmetric stretching vibration

3.2.2 UV laser

PEDOT:PSS/nSi samples were also measured using the UV laser (λ = 325 nm), as shown in Fig. 3(a). In that case, the main Raman modes are observed at ∼1370, 1452, 1530 and 1608 cm^{-1} (inset Fig 3(b)), similarly to the results reported by Lin et al.[42] using a 532 nm laser for PEDOT:PSS with variable concentration of EG(1, 3 or 5%). Vibrational modes between 1200 and 1400 cm^{-1} are commonly assigned to C–C stretch vibrations, while modes between 1400 and 1600 cm^{-1} are related to C=C stretch vibrations, similar to the peak assignation by Du. et al.[39]. Note that the Raman spectra observed in Fig.3 (a), acquired with UV irradiation, differ from those in Fig 2 acquired with the VIS laser, owing to the different excitation source, in fact higher frequency modes are promoted during UV irradiation. Moreover, the PEDOT:PSS layers exhibit a quick degradation under UV laser irradiation, based on the quenching of the total Raman signal observed in Fig.3(a), where Raman spectra were acquired over continuous exposure time using a pinhole of 200 μm and a $0.1 \cdot I_0$ intensity. To monitor the degradation under UV irradiation, in this work we focus on the most intense mode, placed at 1608 cm^{-1}, and its

quenching over time, shown in Fig.3 (b). The minimum Raman intensity is reached after 100-200 s of irradiation, while in most cases only tens of seconds are required to induce a fast intensity decrease. The rate of decrease of the 1608 cm^{-1} mode is faster when using higher excitation energy, as observed in Fig.3(b). However, not every Raman mode evolves in the same way upon irradiation. In Fig. 3(c), the Raman signal was acquired using the VIS laser, after the UV-irradiation, to prevent any further degradation during data acquisition, leading as well to a more defined Raman modes for PEDOT:PSS. Different spots were irradiated using the UV laser during 8 s with variable energy density, as observed in the optical image included as an inset in Fig.3(d) where the spots correspond to: from upper row left to right 0.1, 0.25, 0.5 and I_0 and vice versa for the second row. Higher degradation can be observed in the optical image when increased energy density was employed during measurements. Regarding the corresponding Raman signal, even with short UV irradiation some of the Raman modes (mainly those situated at ∼1499, 1530 cm^{-1}) increase their relative intensity, as shown in Fig.3(c)-(d). In the literature, Toto et al.[22]. demonstrated that PEDOT:PSS can be sensitive to UV-C irradiation. In their work, after prolonged irradiation, a shift of the main peak of PEDOT:PSS towards higher wavenumbers was also detected, which was attributed to the shortening of the conjugation length of the neutral parts in the polymer. Moreover, the remaining modes were also shifted and an increase on the relative intensity of the Raman mode near 1500 and 1530 cm^{-1} was also observed, but not discussed, very similar to our findings (see Fig.3(c)). In our work, the relative intensity of the vibrational modes placed at ∼1499, 1530 cm^{-1} tend to increase upon laser UV irradiation (Fig.3(d)) and a clear change on the appearance was observed in the corresponding optical image acquired after the controlled irradiation (inset in Fig.3(d)). This further supports the idea that UV is inducing changes on the oxidation state of PEDOT. Nonetheless, prolonging the exposure time will quench the total intensity of the Raman signal, as shown in Fig.3(a). Recently laser-induced graphene (LIG) technologies with PEDOT:PSS reported that Raman modes related to PEDOT:PSS could not be detected after laser irradiation [43]. Hence, high control of the irradiation conditions is required either to inhibit or promote PEDOT:PSS degradation on demand. In that sense, the

Raman signal can be monitored to assess the stability of the polymer following the polymer operation conditions, based on potential applications, such as increasing its conductivity.

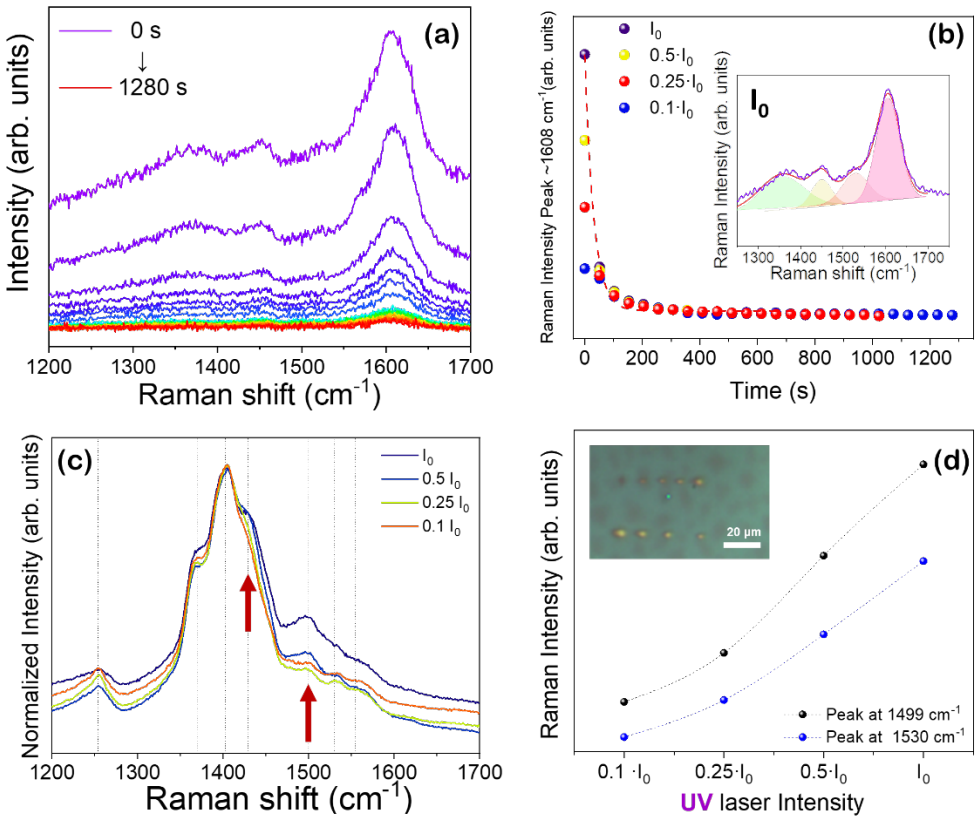

Fig. 3 (a) Quenching of the Raman spectra acquired with the UV laser (λ=325 nm) with pinhole of 200 µm using $0.1 \cdot I_0$ over exposure time. (b) Decrease of the relative intensity of the peak at ~1608 cm^{-1} using different laser irradiation energies (0.1, 0.25, 0.5 and I_0) over UV exposure time. Inset shows deconvolution of the spectra at t=0 with I_0 intensity. (c) Raman spectra acquired with the VIS laser (λ=633 nm) after short time UV laser (λ=325 nm) irradiation with the different UV laser intensities. (d) Increase on the relative intensity of the peaks at ~1499, 1530 cm^{-1} upon laser irradiation intensity due to UV irradiation with variable irradiation energies acquired with the VIS red laser and pinhole of 900 µm. Inset shows optical image from the irradiated spots.

3.3 Etching and aging

The interface between Si/PEDOT:PSS is a matter of study for Si-passivation [9,20] as it plays a major role on its performance. One approach to control the interface consists in modification of the native SiO_X layer, as this affects the passivation behaviour at the junction. Jäckle et al. showed that this oxide layer can grow over time, affecting negatively to the solar cell performance. Therefore, removing this layer could be an efficient approach to improve the photovoltaic performance [20]. To observe the possible influence of this aspect on the passivation performance, in this work the native silicon oxide of the substrate has been removed via a chemical etching, as explained in the Experimental section. Therefore, in this work PEDOT:PSS layers were spin coated on top of either untreated or piranha treated FZ -n Si substrates. Both composites were stored under room conditions for 70 days, and their recombination lifetimes were measured by means of PL-QSSPC as shown in Fig 4(a)-(b). Colour bars beside the PL images indicate the charge carrier lifetime values, which were calculated from the corresponding QSS-PC curves as a function of the injection level. It is important to point out that for measuring correct PL-QSSPC imaging, reflectance of each sample was measured at λ = 808 nm and used as a correction factor. Initially (day 0), lifetime on the composite without etching is around ~300 µs while for the composite with piranha treatment is around ~150 µs (Fig. 4(c)). This is an indicator that removing the oxide layer is not the best approach to obtain better silicon passivation as the native oxide appears to be more stable on the passivation effects, leading to higher lifetime values. Nonetheless, it is important to compare the evolution over time of this lifetime values, as we cannot yet conclude if the removal of the layer will lead to a rapid decrease or not. On the right images (Fig. 4(a), (b)) the pixels with the corresponding carrier lifetime values are presented as a histogram. By comparing the PL degradation over time and the decay trend in the lifetime values (Fig 4(c)), with other works [5,44] it can be observed that the decrease down to ~ 120 µs in 90 days is a trend in agreement with previous reports. The decrease trend comparing treated and untreated samples is similar. Moldarev et al. [44] showed that by placing the substrates in a Nitrogen-filled glovebox the decay is less pronounced. The wafers inside the desiccator show lower degradation but still carrier lifetime decreases. On the contrary, other reports point out that the use of thicker oxide layers increase carrier lifetime [5]. Degradation over time is an unsolved issue and is

commonly ignored in the research literature, despite its key importance on the HSCs performance. Regarding the applicability of these materials as solar cells, IV curves and optical images of the assembled cells (with their corresponding electric contacts) can be observed in Fig S1, while their performance can be observed in Fig. S4.

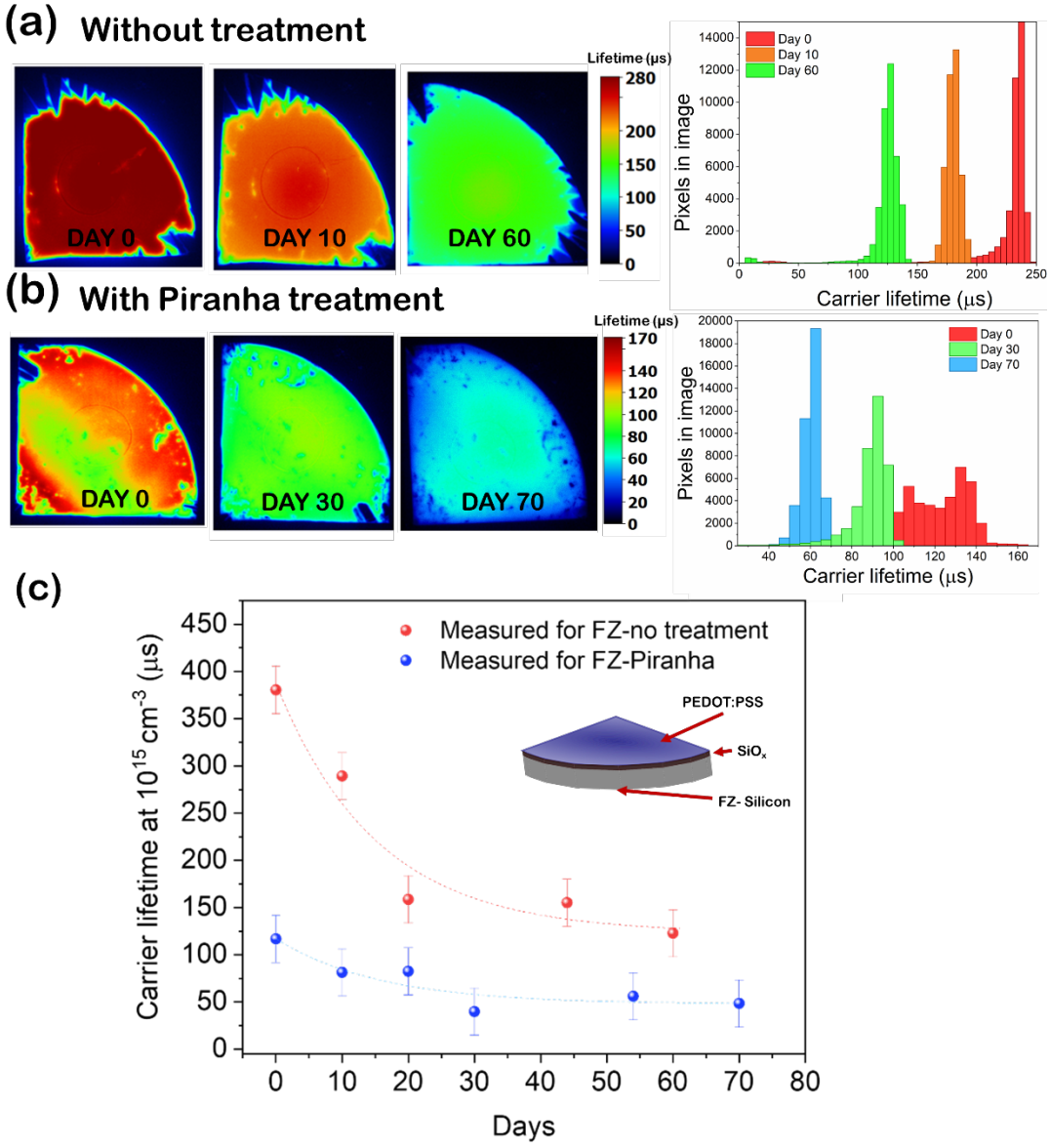

Fig. 4: Decrease over time of the carrier lifetime measured for an injection level of $\Delta n=10^{15}$ cm^{-3} corresponding to the samples deposited over FZ (float zone) n-type Si (a) without treatment and (b) with Piranha treatment. On the right of both images a histogram corresponding to the distribution of pixels near the centre of the sample is shown. (c) shows detailed lifetimes for each sample on different periods of time.

Finally, we can observe the different research items covering the field of PEDOT:PSS. We can clearly observe the importance of PH1000 grade [21,45,46] among different PEDOT:PSS, which is the most common grade employed, shared with PH500 [24–26]. Secondly, we can clearly observe that mostly degradation studies have focused on changes of the electrical conductivity, mostly against thermal treatment [23,45] and with variable atmosphere [25]. Some of those works are included in Table 2 for comparison. As an example, Toto et al [22] studied PEDOT:PSS composites and the influence of UV irradiation, showing a first report on the UV interaction with PEDOT:PSS, while other authors reported the influence of solar irradiation, which tends to decrease the overall performance. As it is known, the overall performance does not depend only on the effect of the electrical conductivity, as other parameters are fundamental for the achievement of an optimal performance. In this work we studied the carrier lifetime recombination, which is an indicator of the solar cell efficiency and the effect of aging. We can observe that it strongly decreases over time, thus limiting the applicability of this solar cells which must be considered.

Table 2: Relevant literature research articles on the topic of PEDOT:PSS degradation.

PEDOT:PSS grade/manufacturer	Thickness (nm)	Substrate	Studied parameter	Variable parameter	Reference
-	45	ITO	Vsc Isc	Time	[47]
Clevios™ PH 500	50	PET	Conductivity	Under temperature	[24]
Clevios™ PH 500	50	PET	Conductivity	Temperature and atmosphere (air and helium)	[25]
P VP Al 4083	50	ITO	Conductivity, surface roughness	Thermal treatment	[23]
Clevios™ PH 1000	100-140	Al_2O_3	Conductivity	Thermal treatment	[45]
Clevios™ PH 1000	26-120	Glass	Resistance	Time (days), thermal treatment, light-dark	[21]
PEDOT:PSS pellets (Orgacon DRY, Sigma-Aldrich)	0.03 mm	Composites	Conductivity, morphology	UV-induced modification of PEDOT:PSS-based nanocomposite (Raman)	[22]
Herraeus PH1000	30-80	Glass or Polyethylene naphthalate (PEN)	Conductivity	Irradiation (light and dark)	[46]

PEDOT:PSS (1.2 wt%)	-	-	Sheet resistance	Thermal treatment	[48]
Clevios™ PH500	Nanometer region	$SiO_2/N^{++}Si$	Conductivity	Aging (atmosphere)	[26]
Clevios™ (Ossila) PH1000	~120	n-type silicon and glass substrates	Carrier recombination Morphology	1. Time (days) 2. UV and Vis laser irradiation 3. Surface oxide etching	This work

4. Conclusions

In this work, degradation effects for the films of PEDOT:PSS/nSi were analysed by different approaches, as the stability of hybrid composites for solar cell applications remains one of the most relevant challenges in this field. Firstly, PEDOT:PSS+DMSO films were spin-coated onto FZ-silicon substrates as candidates for hybrid silicon solar cells. The stability of these composites has been tested with both VIS and UV laser irradiation, aging, and chemical etching of the native oxide layer. Contrary to VIS irradiation, UV laser irradiation leads to a rapid degradation, observed by the quenching of all Raman modes, while when using low exposure time and UV irradiation intensity (8s, 0.1 I_0) changes on the high wavenumber Raman modes were observed due to variation in the PEDOT:PSS molecular arrangement. By using a VIS laser with a high pinhole, changes on the Raman spectra were also detected and discussed. Modifying the PEDOT:PSS/nSi interlayer by removing the native silicon oxide with an acidic etching decreased the recombination lifetime of the silicon substrates, which were even further decreased by continuous aging, reaching lifetime values of 75 s after 400 days, which is a decrease of 78%. While the

recombination lifetimes, conductivity and transparency of PEDOT:PSS-based composites are initially appropriate for photovoltaics applications, there is still room for improvement to overcome the issues regarding its long-term stability over performing conditions, for which this work aimed to give some insights.

Funding

This research was funded by the Spanish Ministry of Innovation, Science, and Technology and the Spanish Ministry of Economy through Research Projects RTI2018-097195-B-I00.

Declaration of Competing Interest

The authors declare that they have no known competing financial interests or personal relationships that could have appeared to influence the work reported in this paper.

Author Contributions:

Conceptualization, A.V.-L., D.M., and A.C.; data curation, A.V.-L. M.G-C, D.M.; formal analysis, A.V.-L.; funding acquisition, A.C.; investigation, A.V.-L., M.G-C; methodology, A.V.-L. M.G-C, D.M.; project administration, D.M., B. M, and A.C; resources, S.Zh.K B. M, and A.C..; software, A.V.-L.; supervision, D.M., S.Zh.K, B.M, A.C.; visualization, A.V.-L., D.M., and A.C.; writing—original draft, A.V.-L.; writing—review and editing, A.V.-L., D.M., S.Zh.K B. M, and A.C. All authors have read and agreed to the published version of the manuscript.

Acknowledgements

Authors thank C.C. You, B. Thomassen and H. Haug for their practical help during measurements at IFE.

References

[1] H. Shi, C. Liu, Q. Jiang, J. Xu, Effective Approaches to Improve the Electrical Conductivity of

PEDOT:PSS: A Review, Adv. Electron. Mater. 1 (2015) 1–16. https://doi.org/10.1002/aelm.201500017.

[2] N.A. Shahrim, Z. Ahmad, A. Wong Azman, Y. Fachmi Buys, N. Sarifuddin, Mechanisms for doped PEDOT:PSS electrical conductivity improvement, Mater. Adv. 2 (2021) 7118–7138. https://doi.org/10.1039/D1MA00290B.

[3] D.Y. Khang, Recent progress in Si-PEDOT:PSS inorganic-organic hybrid solar cells, J. Phys. D. Appl. Phys. 52 (2019) 503002. https://doi.org/10.1088/1361-6463/ab3f64.

[4] X. Jiang, P. Zhang, J. Zhang, J. Wang, G. Li, X. Fang, L. Yang, X. Chen, High Performance of PEDOT:PSS/n-Si Solar Cells Based on Textured Surface with AgNWs Electrodes, Nanoscale Res. Lett. 13 (2018) 53. https://doi.org/10.1186/s11671-018-2462-0.

[5] A. Vázquez-López, M. García-Carrión, E. Hall, A. Yaseen, I. Kalafat, M. Taeño, J. Zhu, X. Zhang, E. Arici, O.S. Taskin, D. Maestre, E. Nogales, P. Hidalgo, J. Ramírez-Castellanos, B. Méndez, N. Yuca, S. Karazhanov, E.S. Marstein, A. Cremades, Hybrid Materials and Nanoparticles for Hybrid Silicon Solar Cells and Li-Ion Batteries, J. Energy Power Technol. 2021, Vol. 3, Page 1. 3 (2021) 1–1. https://doi.org/10.21926/JEPT.2102020.

[6] A. Vázquez-López, A. Yaseen, D. Maestre, J. Ramírez-Castellanos, S.Z. Karazhanov, E.S. Marstein, A. Cremades, Improved silicon surface passivation by hybrid composites formed by PEDOT:PSS with anatase TiO_2 nanoparticles, Mater. Lett. 271 (2020) 127802. https://doi.org/10.1016/j.matlet.2020.127802.

[7] A. Vázquez-López, A. Yaseen, D. Maestre, J. Ramírez-Castellanos, E.S. Marstein, S.Z. Karazhanov, A. Cremades, Synergetic Improvement of Stability and Conductivity of Hybrid Composites formed by PEDOT:PSS and SnO Nanoparticles, Molecules. 25 (2020) 695. https://doi.org/10.3390/molecules25030695.

[8] A. Srivastava, D. Sharma, P. Kumari, M. Dutta, S.K. Srivastava, Highly Efficient PEDOT:PSS/Silicon Hybrid Solar Cells via Effective Surface Microengineering of Low-Cost Solar-Grade Silicon Wafers, ACS Appl. Energy Mater. 4 (2021) 4181–4198. https://doi.org/10.1021/ACSAEM.1C00511/SUPPL_FILE/AE1C00511_SI_001.PDF.

[9] S. Jäckle, M. Liebhaber, C. Gersmann, M. Mews, K. Jäger, S. Christiansen, K. Lips, Potential of PEDOT:PSS as a hole selective front contact for silicon heterojunction solar cells, Sci. Rep. 7 (2017) 1–8. https://doi.org/10.1038/s41598-017-01946-3.

[10] T.R. Chou, S.H. Chen, Y. Te Chiang, T.T. Chang, C.W. Lin, C.Y. Chao, Highly conductive PEDOT:PSS film by doping p-toluenesulfonic acid and post-treatment with dimethyl sulfoxide for ITO-free polymer dispersed liquid crystal device, Org. Electron. 48 (2017) 223–229. https://doi.org/10.1016/J.ORGEL.2017.05.052.

[11] S. Mahato, J. Puigdollers, C. Voz, M. Mukhopadhyay, M. Mukherjee, S. Hazra, Near 5% DMSO is the best: A structural investigation of PEDOT: PSS thin films with strong emphasis on surface and interface for hybrid solar cell, Appl. Surf. Sci. 499 (2020) 143967. https://doi.org/10.1016/j.apsusc.2019.143967.

[12] Y. Xia, S. Dai, Review on applications of PEDOTs and PEDOT:PSS in perovskite solar cells, J. Mater. Sci. Mater. Electron. 1 (2020) 3. https://doi.org/10.1007/s10854-020-03473-w.

[13] K.H. Hwang, D.I. Kim, S.H. Nam, H.J. Seo, J.H. Boo, Study on the effect of DMSO on the changes in the conductivity of PEDOT:PSS, Funct. Mater. Lett. 1 (2015) 1–6. https://doi.org/10.1142/S1793604718500431.

[14] S.-S. Yoon, D.-Y. Khang, Roles of Nonionic Surfactant Additives in PEDOT:PSS Thin Films, J. Phys. Chem. C. 120 (2016) 29525–29532. https://doi.org/10.1021/acs.jpcc.6b12043.

[15] T. Tevi, S.W. Saint Birch, S.W. Thomas, A. Takshi, Effect of Triton X-100 on the double layer

capacitance and conductivity of poly(3,4-ethylenedioxythiophene):poly(styrenesulfonate) (PEDOT:PSS) films, Synth. Met. 191 (2014) 59–65. https://doi.org/10.1016/j.synthmet.2014.02.005.

[16] R. Luo, H. Li, B. Du, S. Zhou, Y. Zhu, A simple strategy for high stretchable, flexible and conductive polymer films based on PEDOT:PSS-PDMS blends, Org. Electron. 76 (2020) 105451. https://doi.org/10.1016/J.ORGEL.2019.105451.

[17] L. Hu, J. Song, X. Yin, Z. Su, Z. Li, Research Progress on Polymer Solar Cells Based on PEDOT:PSS Electrodes, Polymers (Basel). 12 (2020) 145. https://doi.org/10.3390/polym12010145.

[18] J. Chen, Y. Shen, J. Guo, B. Chen, J. Fan, F. Li, B. Liu, H. Liu, Y. Xu, Y. Mai, Electrochemical grafting passivation of silicon via electron transfer at polymer/silicon hybrid interface, Electrochim. Acta. 247 (2017) 826–834. https://doi.org/10.1016/j.electacta.2017.07.071.

[19] D. Zielke, C. Niehaves, W. Lövenich, A. Elschner, M. Hörteis, J. Schmidt, Organic-silicon Solar Cells Exceeding 20% Efficiency, in: Energy Procedia, Elsevier Ltd, 2015: pp. 331–339. https://doi.org/10.1016/j.egypro.2015.07.047.

[20] S. Jäckle, M. Liebhaber, J. Niederhausen, M. Büchele, R. Félix, R.G. Wilks, M. Bär, K. Lips, S. Christiansen, Unveiling the Hybrid n-Si/PEDOT:PSS Interface, ACS Appl. Mater. Interfaces. 8 (2016) 8841–8848. https://doi.org/10.1021/acsami.6b01596.

[21] Y. Shi, Y. Zhou, Z. Che, J. Shang, Q. Wang, F. Liu, Y. Zhou, Degradation phenomena and degradation mechanisms for highly conductive PEDOT:PSS films, Mater. Lett. 308 (2022) 131106. https://doi.org/10.1016/J.MATLET.2021.131106.

[22] E. Toto, S. Botti, S. Laurenzi, M.G. Santonicola, UV-induced modification of PEDOT:PSS-based nanocomposite films investigated by Raman microscopy mapping, Appl. Surf. Sci. 513 (2020).

https://doi.org/10.1016/j.apsusc.2020.145839.

[23] J. Huang, P.F. Miller, J.C. De Mello, A.J. De Mello, D.D.C. Bradley, Influence of thermal treatment on the conductivity and morphology of PEDOT/PSS films, Synth. Met. 139 (2003) 569–572. https://doi.org/10.1016/S0379-6779(03)00280-7.

[24] E. Vitoratos, S. Sakkopoulos, E. Dalas, N. Paliatsas, D. Karageorgopoulos, F. Petraki, S. Kennou, S.A. Choulis, Thermal degradation mechanisms of PEDOT:PSS, Org. Electron. 10 (2009) 61–66. https://doi.org/10.1016/j.orgel.2008.10.008.

[25] E. Vitoratos, Conductivity Degradation Study of PEDOT: PSS Films under Heat Treatment in Helium and Atmospheric Air, Open J. Org. Polym. Mater. 02 (2012) 7–11. https://doi.org/10.4236/ojopm.2012.21004.

[26] D.J. Yun, J. Jung, Y.M. Sung, H. Ra, J.M. Kim, J.G. Chung, S.Y. Kim, Y.S. Kim, S. Heo, K.H. Kim, Y.J. Jeong, J. Jang, In-Situ Photoelectron Spectroscopy Study on the Air Degradation of PEDOT:PSS in Terms of Electrical and Thermoelectric Properties, Adv. Electron. Mater. 6 (2020) 2000620. https://doi.org/10.1002/AELM.202000620.

[27] C. V Amanchukwu, M. Gauthier, T.P. Batcho, C. Symister, Y. Shao-Horn, J.M. D'arcy, P.T. Hammond, Evaluation and Stability of PEDOT Polymer Electrodes for LiO 2 Batteries, J. Phys. Chem. Lett. 7 (2016) 12. https://doi.org/10.1021/acs.jpclett.6b01986.

[28] Y. Dufil, M. Dietrich, D. Zigah, F. Favier, S. Sadki, P. Gentile, O. Fontaine, Y. Dufil, F. Favier, M. Dietrich, P. Gentile, D. Zigah, O. Fontaine, Local Degradation of PEDOT:PSS on Silicon Nanostructures Using Scanning Electrochemical Microscopy, Small. (2022) 2206789. https://doi.org/10.1002/SMLL.202206789.

[29] V. Singh, T. Kumar, Study of modified PEDOT:PSS for tuning the optical properties of its conductive thin films, J. Sci. Adv. Mater. Devices. 4 (2019) 538–543.

https://doi.org/10.1016/j.jsamd.2019.08.009.

[30] J. Liu, J. Niu, D. Yang, M. Yan, J. Sha, Raman spectrum of array-ordered crystalline silicon nanowires, Phys. E Low-Dimensional Syst. Nanostructures. 23 (2004) 221–225. https://doi.org/10.1016/j.physe.2004.03.016.

[31] Y. Huang, Y. Zeng, Z. Zhang, X. Guo, M. Liao, C. Shou, S. Huang, B. Yan, J. Ye, UV-Raman scattering of thin film Si with ultrathin silicon oxide tunnel contact for high efficiency crystal silicon solar cells, Sol. Energy Mater. Sol. Cells. 192 (2019) 154–160. https://doi.org/10.1016/j.solmat.2018.12.025.

[32] S. Nešpůrek, P. Kuberský, R. Polanský, M. Trchová, J. Šebera, V. Sychrovský, Raman spectroscopy and DFT calculations of PEDOT:PSS in a dipolar field, Phys. Chem. Chem. Phys. 24 (2021) 541–550. https://doi.org/10.1039/D1CP03899K.

[33] M. Kong, M. Garriga, J.S. Reparaz, M.I. Alonso, Advanced Optical Characterization of PEDOT:PSS by Combining Spectroscopic Ellipsometry and Raman Scattering, ACS Omega. 7 (2022) 39429–39436. https://doi.org/10.1021/acsomega.2c05945.

[34] P. V Almeida, M.S. Izumi, H.F. Dos Santos, A.C. Sant'ana, SPECTROSCOPIC CHARACTERIZATION OF PEDOT:PSS CONDUCTING POLYMER BY RESONANCE RAMAN AND SERRS SPECTROSCOPIES, Quim. Nov. 42 (1073). https://doi.org/10.21577/0100-4042.20170417.

[35] W.W. Chiu, J. Travaš-Sejdić, R.P. Cooney, G.A. Bowmaker, Studies of dopant effects in poly(3,4-ethylenedioxythiophene) using Raman spectroscopy, J. Raman Spectrosc. 37 (2006) 1354–1361. https://doi.org/10.1002/jrs.1545.

[36] H. Lee, Y. Kim, H. Cho, J. Lee, J.H. Kim, Improvement of PEDOT:PSS linearity *via* controlled addition process, RSC Adv. 9 (2019) 17318–17324. https://doi.org/10.1039/C9RA03040A.

[37] Z. Xu, S. Wang, C. Ma, K. Luo, F. Fang, Effect of Nickel Doping on Phase Transformation of TiO_2 Nanotube Arrays, Phys. Status Solidi. 216 (2019) 1800836. https://doi.org/10.1002/pssa.201800836.

[38] C.S. Pathak, J.P. Singh, R. Singh, Effect of dimethyl sulfoxide on the electrical properties of PEDOT:PSS/n-Si heterojunction diodes, Curr. Appl. Phys. 15 (2015) 528–534. https://doi.org/10.1016/j.cap.2015.01.020.

[39] F.-P. Du, N.-N. Cao, Y.-F. Zhang, P. Fu, Y.-G. Wu, Z.-D. Lin, R. Shi, A. Amini, C. Cheng, PEDOT:PSS/graphene quantum dots films with enhanced thermoelectric properties via strong interfacial interaction and phase separation., Sci. Rep. 8 (2018) 6441. https://doi.org/10.1038/s41598-018-24632-4.

[40] R. Chen, K. Sun, Q. Zhang, Y. Zhou, M. Li, Y. Sun, Z. Wu, Y. Wu, X. Li, J. Xi, C. Ma, Y. Zhang, J. Ouyang, Sequential Solution Polymerization of Poly(3,4-ethylenedioxythiophene) Using V2O5 as Oxidant for Flexible Touch Sensors, IScience. 12 (2019) 66–75. https://doi.org/10.1016/J.ISCI.2019.01.003.

[41] Y. Wang, Y. Dou, Z. Wu, Y. Tian, Y. Xiong, J. Zhao, D. Fang, F. Huang, Y.B. Cheng, J. Zhong, Ultrafast-laser-treated poly(3,4-ethylenedioxythiophene): poly(styrenesulfonate) electrodes with enhanced conductivity and transparency for semitransparent perovskite solar cells, Front. Chem. Sci. Eng. (2022) 1–11. https://doi.org/10.1007/S11705-022-2203-X/.

[42] Y.J. Lin, W.S. Ni, J.Y. Lee, Effect of incorporation of ethylene glycol into PEDOT:PSS on electron phonon coupling and conductivity, J. Appl. Phys. 117 (2015) 1–5. https://doi.org/10.1063/1.4921930.

[43] Z. Chu, C. Liu, Y. Lu, Laser-induced porous graphene from PEDOT:PSS films for dye-sensitized solar cells, Mater. Lett. 323 (2022) 132537. https://doi.org/10.1016/J.MATLET.2022.132537.

[44] D. Moldarev, M. Taeño, D. Maestre, A. Cremades, S.Z. Karazhanov, E. Marstein, Electrical and optical properties of composite PEDOT:PSS-based thin films with NiO nanoparticles, Mater. Today Proc. (2020). https://doi.org/10.1016/j.matpr.2020.04.549.

[45] L. Stepien, A. Roch, R. Tkachov, B. Leupolt, L. Han, N. van Ngo, C. Leyens, Thermal operating window for PEDOT:PSS films and its related thermoelectric properties, Synth. Met. 225 (2017) 49–54. https://doi.org/10.1016/j.synthmet.2016.11.017.

[46] A. Schultheiss, M. Gueye, A. Carella, A. Benayad, P. Pouget, M. Faure-Vincent, R. Demadrille, A. Revaux, J.-P. Simonato, Insight into the Degradation Mechanisms of Highly Conductive Poly(3,4-ethylenedioxythiophene) Thin Films, ACS Appl. Polym. Mater. 2 (2020) 2686–2695. https://doi.org/10.1021/acsapm.0c00301.

[47] V. Singh, S. Arora, M. Arora, V. Sharma, R.P. Tandon, Characterization of doped PEDOT: PSS and its influence on the performance and degradation of organic solar cells, Semicond. Sci. Technol. 29 (2014) 045020. https://doi.org/10.1088/0268-1242/29/4/045020.

[48] J.L. Carter, C.A. Kelly, M.J. Jenkins, Processing optimization of PEDOT:PSS and PEDOT:PSS/Tween 80 films, Polym. J. 2022. (2022) 1–8. https://doi.org/10.1038/s41428-022-00740-x.